KINEMATIC DESIGN OF A THREE DEGREE OF FREEDOM PARALLEL HAND CONTROLLER MECHANISM

Bernard D. Adelstein[§‡]**, Peter Ho**[‡]**, and H. Kazerooni**[‡]

[§]NASA Ames Research Center
Moffett Field, CA 94035

[‡]Mechanical Engineering Department
University of California, Berkeley, CA 94720

ABSTRACT

This paper presents the kinematic design of a 10 link "in-parallel" mechanism for use in a three degree of freedom force-reflecting haptic interface. The mechanism linkage couples three coplanar rotary electric motor shafts to the endpoint grasped by the human operator. The linkage permits all motor housings to be supported on a common base, thereby reducing the inertia and weight that the interface actuators and human operator must support and move. Furthermore, because only rigid links and rotary ball bearings are used, the linkage avoids the compliance, friction, and/or backlash associated with other types of transmission elements. The linkage workspace is bounded by the singular sphere of maximum reach and separated into two hemispheres by singularities in the plane of the motor shafts.

1. INTRODUCTION

1.1 Haptic Perception and Display

Haptic perception is the process through which we explore and evaluate the physical characteristics (*e.g.*, size, weight, shape, stiffness, viscosity, temperature, *etc.*) of objects or fields (*e.g.*, gravity) in our immediate surroundings. Haptic perception of *mechanical* characteristics involves the cognitive integration of sensory input from strain (length), strain rate (velocity), and force sensors in the muscles and joints, as well as normal and shear pressures from tactile sensors in the skin induced by direct interaction between our limbs and the environment. In the work described here, we are concerned with the type of mechanical inputs intended specifically to stimulate the muscle and joint sensors.

Haptic displays that are designed to stimulate the muscle senses combine both force-reflecting interface hardware and a computation engine. The interface hardware typically consists of a mechanical linkage in the form of a joystick or exoskeleton that joins the human operator to a source of mechanical power—either electromagnetic, electrohydraulic, or electropneumatic actuators. Because of this external coupling at the skin, a force reflecting interface that stimulates the human limb and muscle sense of physical dynamics, either by default or by design, also affects the tactile sensors in the skin. For virtual environments (VE), the computation engine governs the behavior of the actuators and linkage as a function of kinematic and force measurements from interface transducers, according to algorithms and equations that describe the models to be simulated. In telemanipulation, the computer still modulates interface behavior, but the model is now either replaced or augmented by transducer information from the remote site.

1.2 Historical Perspective

The first electrically powered force reflecting displays, developed in the late 1940's for the remote handling of nuclear materials, employed master and slave arms that were kinematic replicas of each other and thus permitted simple analog electronic control without digital computation (Goertz and Thompson, 1954). One offshoot of these kinematic replica systems was the prototype man amplifier of the mid 1960's in which the operator donned a master exoskeletal linkage which itself was encased by an electrohydraulically powered slave linkage (Mosher, 1967). Sutherland (1965) first suggested that data generated or stored in a computer (*i.e.*, digital simulations), could drive the forces applied to the human by these exoskeletons or "wearable joysticks." The first force displays of computer simulations were demonstrated in the late 1960's (Noll, 1971; Batter and Brooks, 1971) on simple two and three degree of freedom (dof) joysticks that were not worn. By the mid 1970's, Brooks (1977) and colleagues were using a force reflecting master arm to display six dof forces from computer simulations.

1.3 Haptic Interface Configurations

The growing interest in force reflecting interfaces—as display channels for VEs, as master hand controllers for full and micro scale telemanipulation, and as research tools for studying passive arm dynamics, haptic perception, and manual control—has prompted a broad array of haptic display designs. A sample of more recent developments include a seven dof electrohydraulic exoskeleton arm (Jacobsen et al., 1991), glove mounted electropneumatic cylinders to interact with palm, thumb, and fingers (Burdea et al., 1992), several electromechanical (*i.e.*, electric motor) exoskeletons (Jau, 1991; Bergamasco et al., 1995), and the growing list of electromechanically actuated joystick devices expanded upon below.

The simplest electromechanical joystick linkage configuration, called "direct-drive," locates each actuator directly at the joint between a pair of adjacent links—the proximal link (the one closer to the base) attached to the actuator's fixed element (*i.e.*, stator) and the distal link attached directly to the actuator's moving element (*i.e.*, rotor). While direct-drive can offer the nearest to ideal *passive* dynamics for a single dof interface, multiple dof direct-drive configurations necessitate that the requisite number of single dof actuators be mounted "in-series"—*i.e.*, each motor's distal link serves as the proximal link for the next actuator in the serial chain. The disadvantage of each link having to carry and *move* the inertia and weight of the next joint's actuator is the need for larger actuators and stiffer—and therefore more massive proximal—links. This, in turn, further increases inertia and weight.

Examples of electromechanical joystick interfaces that are at least in part serial include devices described by Jacobus et al. (1992), Ellis et al. (1993), and Massie and Salisbury (1994). An interesting counterexample, developed by Salcudean et al. (1995), is a true direct-drive device that employs a single six dof actuator and does not resort to serial linkages.

In nearly all current multi-dof haptic interfaces, the weight and inertia problems associated with serial direct drive configurations are alleviated to some degree by incorporating transmission elements between one or more motors and the point of attachment to (or grasp by) the human operator. Transmissions serve to transform rotary into rectilinear motion, reduce speed and multiply force (or vice versa), and transfer motion and force from one location in the linkage to another. By introducing transmissions of the various forms described below, actuators may be located remotely from the joints that they drive. In some joystick interfaces, transmission elements allow *all* actuators to be mounted on a common base link or ground, thereby reducing significantly the weight and inertia that must be carried and thus decreasing the power requirements and size for the actuators.

One class of transmission includes "higher pair" kinematic elements such as gears (*e.g.*, Jacobus, et al. 1992) and cables or tendons (*e.g.*, Lindemann and Tesar 1989; Hirata and Sato, 1992; Ellis, et al., 1993; Massie and Salisbury, 1994; Hayward 1995).

The second type of transmissions between actuators and endpoint is composed of closed loop chains of lower kinematic pairs—*i.e.*, linkages with revolute, prismatic, or spherical joints.[1]

---

[1] These joints are lower pairs only *in principle* because practical implementation typically relies on ball or other rolling contact anti-friction bearings which are higher pair elements.

Examples of closed chain joystick mechanisms, termed "in-parallel" or "parallel" (as opposed to "in-series" or "serial") configurations, include two dof planar five bar (Faye, 1986; Ramstein and Hayward, 1994) and seven bar planar linkages (Kazerooni, 1995; Buttolo and Hannaford, 1995); five bar spherical linkages (Adelstein and Rosen, 1992); planar three dof linkages (Millman et al., 1993); and spatial three dof (Hui et al., 1995) and six dof Stewart platform variants (Iwata, 1990; Marshall et al., 1993; Hunter et al., 1994).

In this paper, we present the kinematic description of a new "parallel" spatial linkage that forms the basis of a three dof force-reflecting haptic interface that we are now building.

2. DESIGN OBJECTIVES

The haptic interface whose kinematic design we discuss in this paper is intended initially for manual control research in a three dimensional coordinated haptic-visual virtual environment. For work in a *three* dof haptic environment, in which the purpose of the interface is the display of mechanical dynamics explicitly for muscle sensory organs, we chose to develop a device capable of the minimum necessary number of dofs. These three dofs correspond to translational displacements (as seen in the immersing VE visual display) and forces at the human-machine interface and will not include orientation angles and torques. Thus, all interactions at the human-machine interface will occur through a single point where only forces, as opposed to arbitrary rigid body moments or couples, can be applied. By restricting the interface to three dofs, we reduce design and implementation complexity associated with higher dof devices.

The haptic interface workspace will be sized to conform with the displacement region over which binocular stereo vision is a significant contributor to human visual depth perception. This depth range coincides with the normal extent of human arm motion in the midsagittal plane—*i.e.*, the 60 cm (24 in) or so beginning from ~15 cm (6 in) in front of the nose up to full arm reach. Our intent is to have at minimum a 15 cm spherical well conditioned manual workspace centered in this region.

Other performance objectives not addressed in this paper, but that we are considering in the design of this three dof haptic interface, include interface bandwidth and force dynamic range—the ratio of maximum continuous force to minimum force threshold and resolution due to friction and ripple. In this paper, discussion is limited to the interface kinematics that arise from the components and configuration selected to help meet these objectives

The haptic interface that we are developing has electromechanical actuators. Due to reasons of cleanliness and portability, electrohydraulic actuation was ruled out as a mechanical power source. Unacceptable mechanical compliance precluded the use of electropneumatic actuation for this work. Furthermore, to reduce design complexity, we elected to build a fixed-base joystick-type device.

3. LINKAGE MODEL AND OPERATION

The haptic interface that we are developing is based on the three dof, 10-link, 12 revolute-joint (12R) mechanism, depicted in the three panels of Fig. 1. The linkage shown in Fig. 1 is a *kine-*

matic model—*i.e.*, the link lengths, link angles, and joint placements are, in general, chosen for convenience of illustration and are not necessarily those that optimize the device's workspace characteristics, structural properties, or manufacturability. Specific restrictions on these link geometric parameters are discussed below.

Rotary actuators in the mechanism, labeled *A*, *B*, and *C*, are attached to a common ground link (link 1). These actuators can drive, and be backdriven, by the spherical grip *D* in three spatial degrees of freedom. Each rigid link (numbered 2 through 10, plus ground link 1) is paired to its neighbors by single dof rotary joints (represented by the wheels and hubs). In addition, links 5, 2, and 8 are extensions to the shafts of the motors *A*, *B*, and *C* respectively, that, in principle, can use the motor bearings for their individual joints with ground link 1. Thus all mechanism force and motion is transferred through transmissions made of rigid links and single dof rotary ball bearing joints with very low friction and backlash.

The "flat" depiction provided in Fig. 2 shows all links and joints of the 10 link 12R mechanism. The mechanism is arranged in three adjoining closed loops (*I*, *II*, *III*), with each loop composed of three ternary (three joint) links and a pair (dyad) of binary (two joint) links. Link 5 at the center is common to all three loops; the other ternary links (1, 6, and 4) are only shared between adjacent loops.

The interface mechanism has two major components. The first component, the two loop (loops *I* and *II* in Fig. 2) mechanism base, is the three dof spherical 8-link, 9-joint, linkage shown separately in Fig. 3. It is termed spherical because the axes through all joints between links 1 through 8 intersect at a common center point, as would lines drawn normal to the surface of a hypothetical sphere. The second component (loop *III* in Fig. 2) is a planar closed chain formed by the addition of links 9 and 10 and the extension of links 4 and 6 from the configuration in Fig. 3 to the configuration shown in Fig. 1. The planar linkage (links 4, 5, 6, 9, and 10), in which all joint axis lines are always parallel, allows the endpoint *D* to be moved radially inward and outward with respect to the spherical center of the mechanism. While "parallel" spherical linkages for generating three dof orientation have been designed and analyzed (Gosselin and Angeles, 1989; Marco, Torfason, and Tesar, 1989), the different ternary link placement in the spherical portion of this mechanism permits attachment of the planar loop and therefore allows three dof *spatial* motion.

To understand how the linkage operates, consider locking any two of the three actuator shafts—*i.e.*, any two of links 5, 2, and 8—at a time with respect to ground (link 1). Starting with all three actuators locked, freeing up *A*, enables only links 5, 6, 4, 7, 9, and 10 (shaded components in Fig. 1a) to move, resulting in endpoint *D* motion along arc *a-a*. Similarly, releasing *B* while locking *A* and *C* allows movement exclusively of links 2, 3, 4, 9, and 10 (shaded components in Fig. 1b) and hence, motion of endpoint *D* along arc *b-b*. Freeing actuator *C* alone, permits motion of only links 8, 7, 6, 9, and 10 (shaded components in Fig. 1c), resulting in endpoint arc *c-c*. Thus, when all three actuator shafts are free to rotate, it can be seen that the three arcs, *a-a*, *b-b*, and *c-c* sum to permit three dimensional motion at *D*.
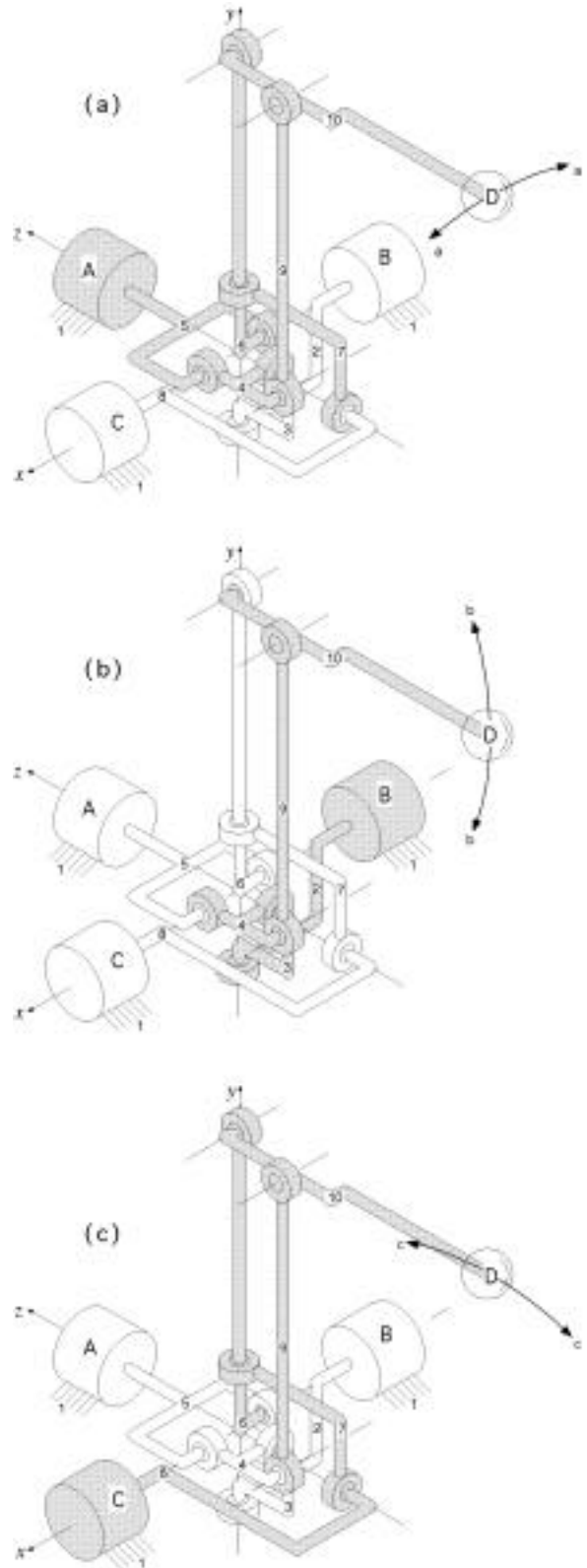

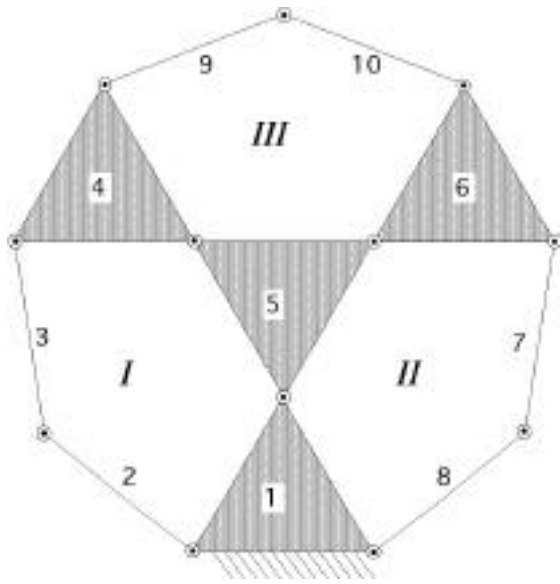**Figure 1.** 10 Link 12R mechanism with different actuators enabled.

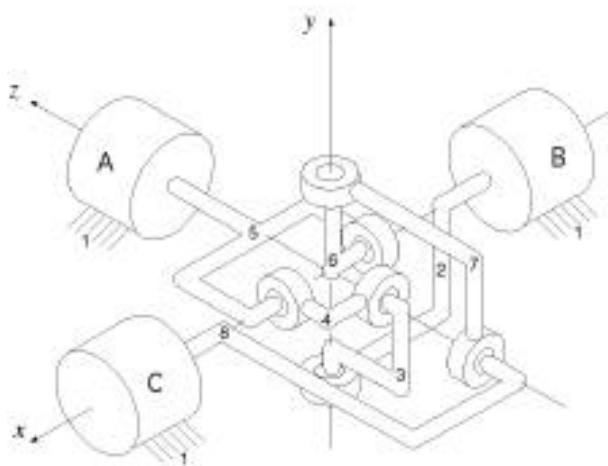**Figure 2.** Planar equivalent 10 Link 12R mechanism.

Figure 3. Eight link spherical portion of mechanism.

4. LINKAGE RESTRICTIONS

Implementation of the 10-link 12R mechanism depends only on meeting the following two constraints: 1) loops *I* and *II* (links 1 through 8) form a spherical linkage—*i.e.*, all joint axes intersect at a common center; and 2) loop *III* (links 4, 5, 6, 9, and 10) forms a planar linkage—*i.e.*, all joint axes are parallel. To satisfy simultaneously the spherical and planar loop constraints, the axes of the joints 4-5 (between links 4 and 5) and 5-6 (between links 5 and 6) must be collinear. In general, subject to these constraints and to requirements for individual loop closure, the spherical links can subtend any arbitrary angle between adjacent joints and the planar links can have any arbitrary length. Arbitrary link lengths and angles, however, can significantly complicate descriptions of linkage kinematics—*i.e.*, the equations relating actuator *A*, *B*, and *C* shaft angles with displacement of endpoint *D*.

For the link lengths and angles shown in Figs. 1 and 3, development of the closed form kinematic relations is straightforward. In this preferred configuration, axis *A* is orthogonal to the collinear axes of *B* and *C*. Additionally, within the eight links comprising the spherical mechanism isolated in Fig. 3, each joint axis (with the exception of joints 4-5 and 5-6 discussed above) is oriented at 90 degrees with respect to the axis of its neighboring joint in its link. Thus, in the "nominal" configuration depicted by Figs. 1 and 3, all bearing axes in the spherical portion of the linkage, including those of the actuators, lie along the three principal orthogonal axes (*i.e.*, *x-y-z* Cartesian coordinates) fixed with respect to ground (link 1). Furthermore, the link lengths of the planar portion (loop *III*) form a parallelogram—*i.e.*, link 6 is equal in length to link 9, and link 4 is equal in length to the portion of link 10 within loop *III*.

5. LINKAGE KINEMATICS

5.1 Forward Geometry

The derivation of the 10 link 12R mechanism's kinematic expressions relating actuator *A*, *B*, and *C* shaft angles (α, β, and γ respectively) and endpoint displacements in the base *x-y-z* Cartesian coordinate system is carried out by considering loops *I*, *II*, and *III* separately and then combining results across shared links.

Starting with the spherical portion of the mechanism in Fig. 3, we cut link 5 to arrive at the spherical five-bar linkage for loop *I* (links 1-5 and actuators *A* and *B*) shown in Fig. 4. The analysis proceeds by further dividing the five-bar closed chain into two separate serial chains. The first chain has link 5, which rotates through angle α about axis z_A fixed to ground (link 1), and link 4 which rotates through angle β_3 about axis z_B fixed to the distal end of link 5. The second chain has links 2 and 3, which rotate through angles β and β_1 about axes z_B and z_B respectively.

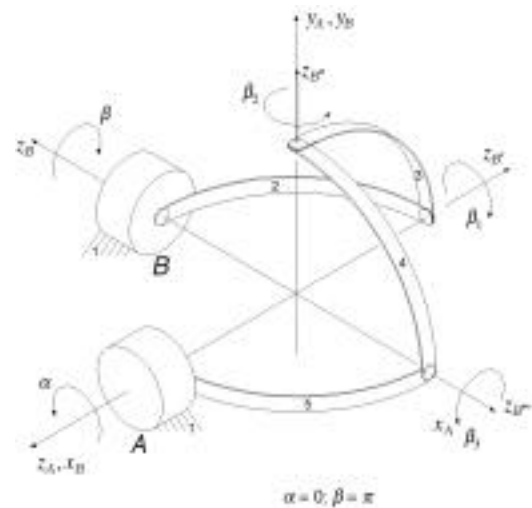**Figure 4.** Spherical 5 bar subset (loop *I*) of 10 Link 12R mechanism.

The axis z_B which has direction $\mathbf{x}_B = \begin{bmatrix} 0 & 0 & 1 \end{bmatrix}^t$ in the coordinate frame fixed to the distal end of link 4 can be transformed into the base frame of z_A by following the path of the first chain according to

$$\mathbf{x}_A = \left(\mathbf{T}_A^B \ \mathbf{T}_B^B \right) \mathbf{x}_B \qquad (1)$$

where

$$\left(\mathbf{T}_A^B \ \mathbf{T}_B^B \right) = \begin{array}{cccccc} 0 & -s\alpha & c\alpha & 0 & -s\beta_3 & c\beta_3 \\ 0 & c\alpha & s\alpha & 0 & c\beta_3 & s\beta_3 \\ -1 & 0 & 0 & -1 & 0 & 0 \end{array} \qquad (2)$$

and $c\alpha = \cos(\alpha)$, $s\alpha = \sin(\alpha)$, *etc.*

Substituting Eq. (2) into Eq. (1) yields, in terms of the first chain's rotations,

$$\mathbf{x}_A = \begin{bmatrix} -s\alpha s\beta_3 & c\alpha s\beta_3 & -c\alpha \end{bmatrix}^T \qquad (3)$$

In the same manner, the direction of axis z_B can be transformed by the second chain's rotations into the frame of z_B:

$$\mathbf{x}_B = \begin{bmatrix} -s\beta s\beta_1 & c\beta s\beta_1 & -c\beta \end{bmatrix}^T \qquad (4)$$

Transforming $\mathbf{x}_B$ into the z_A coordinate frame by the rotation

$$\mathbf{x}_A = \begin{array}{ccc} c(\pi/2) & 0 & s(\pi/2) \\ 0 & 1 & 0 \\ -s(\pi/2) & 0 & c(\pi/2) \end{array} \mathbf{x}_B \qquad (5)$$

allows Eq. (4) to be expressed as

$$\mathbf{x}_A = \begin{bmatrix} -c\beta & c\beta s\beta_1 & s\beta s\beta_1 \end{bmatrix}^T \qquad (6)$$

Solving for the three unit direction components of the z_B axis direction in the $x_A y_A z_A$ coordinate system, *i.e.*, $\mathbf{x}_A = [e_x \ e_y \ e_z]^t$ of Eqs. (3) and (6), subject to the normalization constraint

$$e_x^2 + e_y^2 + e_z^2 = 1 \qquad (7)$$

eliminates β_1 and β_3 and yields

$$e_x = \mp \left(s\alpha c\beta \right) / d_\beta \qquad (8)$$

$$e_y = \pm \left(c\alpha c\beta \right) / d_\beta \qquad (9)$$

$$e_z = \pm \left(c\alpha s\beta \right) / d_\beta \qquad (10)$$

where $d_\beta = \left(1 - s_\alpha^2 s_\beta^2 \right)$.

The direction of the z_C axis for spherical loop *II* (links 5-6-7-8-1) can be derived in the same manner, producing relations similar to Eqs. (8), (9), and (10), except with replacement of angle β by γ —the angle between link 8 and ground.

The combined extension of the links 6 and 10 can then be determined from the two spherical loop directions, z_B and z_C. Since loop *III* (links 4, 5, 6, 9, and 10) forms a parallelogram, link 10 is always parallel to z_B, the joint axis direction between links 3 and 4 seen in Figs. 1 and 3. The direction of link 6 corresponds to z_C for the joint between links 6 and 7. Thus, the displacement of endpoint D in the coordinate system of Fig. 1, found by summing vectorially link 6 with length L_1 and link 10 with length L_2 is:

$$x = -\left[L_1 \left(s\alpha c\beta \right) / d_\beta + L_2 \left(s\alpha c\gamma \right) / d_\gamma \right] \qquad (11)$$

$$y = \left[L_1 \left(c\alpha c\beta \right) / d_\beta + L_2 \left(c\alpha c\gamma \right) / d_\gamma \right] \qquad (12)$$

$$z = \left[L_1 \left(c\alpha s\beta \right) / d_\beta + L_2 \left(c\alpha s\gamma \right) / d_\gamma \right] \qquad (13)$$

where $d_\beta = \left(1 - s_\alpha^2 s_\beta^2 \right)$ and $d_\gamma = \left(1 - s_\alpha^2 s_\gamma^2 \right)$

5.2 Inverse Geometry

The inverse linkage geometry describes actuator angles α, β, and γ as functions of endpoint coordinates x, y and z. As is typical for closed chain mechanisms, the inverse kinematics, even when derivable in closed form, are considerably more involved than the forward description.

Dividing Eq. (11) by Eq. (12) gives the only straightforward result,

$$\alpha = -\tan^{-1} \frac{x}{y} \qquad (14)$$

Considerable manipulation of Eqs. (11), (12), and (13) yields

$$\beta = \cos^{-1} \pm \sqrt{\frac{-Q \pm \sqrt{Q^2 - 4PR}}{2P}} \qquad (15)$$

where

$$P = f^2 + g^2$$

$$Q = 2fh - g^2$$

$$R = h^2$$

in which

$$f = \left(x^2 + y^2 \right)^2 - Ux^2 - y^2 z^2$$

$$g = 2\left(x^2 + y^2 \right) yz$$

$$h = \left(z^2 - U^2 \right) y^2$$

and

$$U = \frac{x^2 + y^2 + z^2 + L_1^2 - L_2^2}{2L_1}$$

The values for β derived from Eq. (16) are then used to solve

$$\gamma = \cos^{-1} \pm \sqrt{\frac{y^2 V^2}{L_2^2 - x^2 V^2}} \qquad (16)$$

in which

$$V = 1 - \frac{L_1 c\beta}{\sqrt{x^2 c^2 \beta + y^2}}$$

5.3 Instantaneous Kinematics

The forward Jacobian, $\mathbf{J} = d\mathbf{x}/d\mathbf{q}$, relating instantaneous actuator motion in configuration space (α, β, γ) to Cartesian motion of linkage endpoint D, found by partial differentiation of Eqs. (11), (12), and (13), is

$$\mathbf{J} = \frac{1}{d_\beta^3 d_\gamma^3} \begin{matrix} -\left(L_1 d_\gamma c\alpha c\beta + L_2 d_\beta c\alpha c\gamma\right) & L_1 d_\gamma s\alpha c^2 \alpha s\beta & L_2 d_\beta s\alpha c^2 \alpha s\gamma \\ -\left(L_1 d_\gamma s\alpha c^3 \beta + L_2 d_\beta s\alpha c^3 \gamma\right) & -L_1 d_\gamma c^3 \alpha s\beta & -L_2 d_\beta c^3 \alpha s\gamma \\ -\left(L_1 d_\gamma s\alpha s\beta c^2 \beta + L_2 d_\beta s\alpha s\gamma c^2 \gamma\right) & L_1 d_\gamma c\alpha c\beta & L_2 d_\beta c\alpha c\gamma \end{matrix} \qquad (17)$$

Because of the unwieldiness of the analytic expression for $\mathbf{J}^{-1}$, quantification of the inverse instantaneous motion is carried out more easily by inverting numerically the 3-by-3 Jacobian of Eq. (17) for each set of (α, β, γ) actuator angle values.

5.4 Kinematic and Static Singularities

Kinematic and static singularities of the 10 link 12R mechanism are given by the Jacobian determinant

$$\det(\mathbf{J}) = \frac{L_1 L_2 c^3 \alpha s(\beta - \gamma)}{d_\beta^3 d_\gamma^3} \times \left[L_1 c\beta/d_\beta + L_2 c\gamma/d_\gamma\right]. \qquad (18)$$

Kinematic singularities at which one or more output dofs is lost—*i.e.*, when infinite instantaneous motion in (α, β, γ) results in no motion in one or more output coordinates—occur for the three conditions when $\det(\mathbf{J}) = 0$. These conditions are:

$$c\alpha = 0 \quad (i.e., \ \alpha = \pi/2)$$

for which endpoint D is in the x-z plane;

$$s(\beta - \gamma) = 0 \quad (i.e., \ \beta = \gamma \ or \ \beta = \gamma \pm \pi)$$

for which links 6 and 10 are collinear because the planar linkage is either fully extended to maximum reach or fully folded in on itself; and

$$\left[L_1 c\beta/d_\beta + L_2 c\gamma/d_\gamma\right] = 0$$

which from Eqs. (11) and (12) corresponds to endpoint D on the line $x = y = 0$, *i.e.*, on the z axis. For the special case $L_1 = L_2 = L$, kinematic singularities of the linkage lie only in the x-z plane and on the sphere of maximum linkage reach (*i.e.*, when $\beta = \gamma$).

Static singularities, when $\det(\mathbf{J})$, are mechanism configurations in which actuators at the base cannot resist certain moments or force applied to the linkage and maintain all links in static equilibrium (Ouerfelli and Kumar, 1994). The static singularities of Eq. (15) arise when $d_\beta = 0$ (*i.e.*, *both* $\alpha = \pi/2$ and $\beta = \pi/2$) or when $d_\gamma = 0$ (*i.e.*, *both* $\alpha = \pi/2$ and $\gamma = \pi/2$) which again corresponds to endpoint D in the x-z plane.

Thus, for link lengths $L_1 = L_2 = L$, the maximum workspace attainable by the 10 link 12R mechanism is spherical in shape with radius $L_1 + L_2 = 2L$, and is divided in half by singularities in the plane of the actuator shafts. The actual reachable workspace will of course be subject to further restrictions imposed by internal linkage interference.

By comparison, the standard *serial* three dof spherical linkage (a fixed-base revolute joint perpendicular to the x-z plane, upon which is mounted a two dof arm whose revolute joint axes are always parallel to the x-z plane) has the same singular maximum spherical reach. For the case of equal length arm links, $L_1 = L_2 = L$, the standard serial linkage's only singularities within this sphere are collinear with the rotational axis of the base actuator.

5.5 Condition Number

The Jacobian condition number, $c(\mathbf{J})$, a measure of the isotropy of the ellipsoid associated with the matrix $\mathbf{J}\mathbf{J}^T$, has been used in kinematic linkage design to predict output force magnitude for fixed actuator power and as an indicator of force/velocity error propagation characteristics (*e.g.*, Salisbury and Craig, 1982; Gosselin and Angeles, 1989; Ouerfelli and Kumar, 1994). Smaller condition number magnitude thus enhances linkage performance at a particular workspace location, with the optimum corresponding to the isotropic ellipsoid for the minimum value of $c(\mathbf{J}) = 1$.

Plots of $c(\mathbf{J})$ for the 10 link 12R linkage with normalized link lengths, $L_1 = L_2 = 1$, are shown in Fig. 5. Note that the condition number for this mechanism are symmetric across the x-z and x-y planes. Optimal values of $c(\mathbf{J})$ for the octant plotted in Fig. 5 occur only in the $x = 0$ plane (*i.e.*, $\alpha = 0$), at $y = z = 1$ (either $\beta = 0$ and $\gamma = \pi/2$, or $\beta = \pi/2$ and $\gamma = 0$).
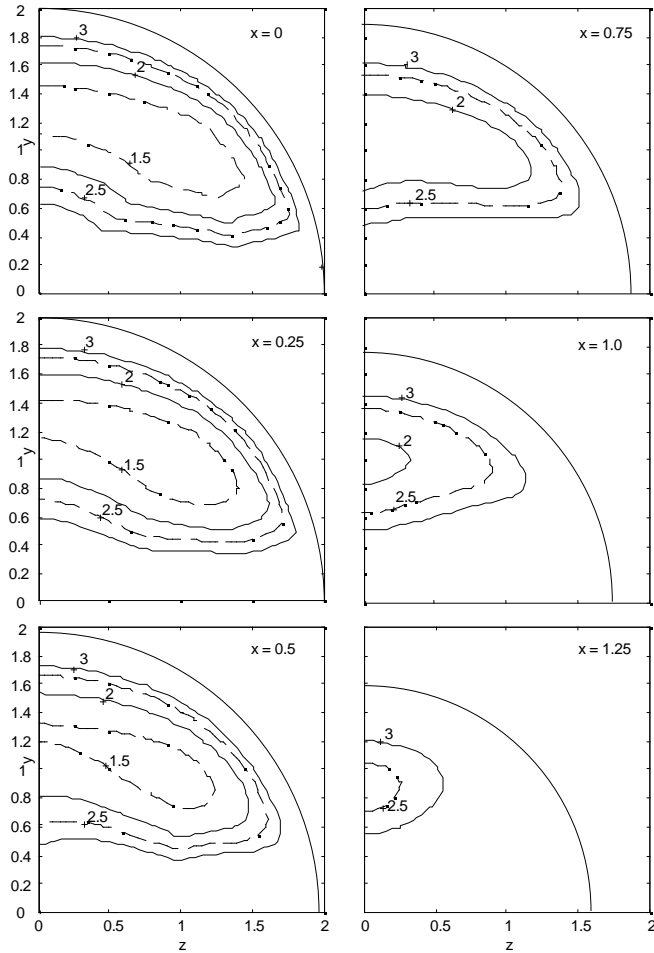
Figure 5. Condition number $c(\mathbf{J}^I)$ for 10 Link 12R mechanism for slices x = 0.0, 0.25, 0.5, 0.75, 1.0, and 1.25. The heavy gauge arc corresponds to the maximum reach in the respective x plane. Note that the quarter plane $y,z \ge 0$ in each slice is symmetric about both y and z axes.

Based on a criterion of $c(\mathbf{J}) < 3.0$ for a "well conditioned" workspace, the contours of the plots in Fig. 5 place the tightest constraint on the y-component, which is at maximum 1.2 units thick. Using this normalized dimension, we selected linkage lengths of $L_1 = L_2 = 15$ cm to accommodate our minimum objective of a 15 cm (6 in) spherical workspace. With this scaling, the contours in Fig. 5 demonstrate that the region for $c(\mathbf{J}) < 3.0$ is as much as 18 cm (7 in) in the y dimension, 54 cm (21 in) in the z dimension, and at least 37.5 cm (14 in) in the x dimension.

6. CONCLUSION

This paper has presented the kinematics of a parallel 10 link, 12 revolute joint, three dof linkage that we are developing for use in a force reflecting haptic display. This linkage allows displacements and forces at the endpoint to be coupled to the rotations and torques at three actuators whose stators are fixed to a common base link. Because all actuators are mounted at ground, none of the housing and stator weight and inertia needs to be carried, and, consequently, actuator and linkage size requirements are reduced. Decreased inertia will increase the structural bandwidth of the linkage, which, in turn, can be expected improve controller bandwidth and performance.

Because the linkage is composed solely of revolute joints and rigid links, it accomplishes the coupling between actuators and endpoint without resorting to spherical pair (*i.e.*, ball) joints, gears, belts, cables, lead/ball screws or other transmission elements. Since a force-reflecting interface depends on accurate actuation and measurement for purposes of control, improvement to the passive linkage's transmission characteristics (by minimizing backlash, friction, and compliance) would be expected to enhance the performance of the controlled device.

These improved transmission characteristics are especially critical to the design of force-reflecting interfaces in which undesirable inertia, compliance, backlash and friction easily felt by the operator can hinder both the quality of haptic information transfer to the human and the accuracy of human generated command inputs.

REFERENCES

Adelstein, B.D., and Rosen, M.J., 1992, "Design and Implementation of a force reflecting manipulandum for manual control research," *Advances in Robotics,* DSC-Vol 42, ASME, New York, pp. 1-12.

Batter, J.J., and Brooks, Jr., F.P., 1971, "A computer display to the sense of feel," *Information Processing 1971, Proceedings, IFIP Congress 71*, Ljubljana, pp. 506-508.

Bergamasco, M., Allota, B., Bosio, L., Ferreti, L., Prisco, G.M., Parrini, Salsedo, F., and Sartini, G., 1994, "An arm exoskeleton system for teleoperation and virtual environment applications," *Proceedings, IEEE Int. Conf. Robotics and Automation*, San Diego, CA, pp. 1449-1454.

Brooks, F.P., 1977, "The computer 'scientist' as toolsmith—studies in interactive computer graphics," *Proceedings, IFIP Congress 77*, Toronto, pp. 625-634.

Burdea, G., Zhuang, J., Roskos, E., Silver, D., and Langrana, N., 1992, "A portable dexterous master with force feedback," *Presence*, 1, pp. 18-28.

Buttolo, P., and Hannaford, B., 1995, "Advantages of actuation redundancy for the design of haptic displays," *Proceedings, ASME Dynamic Systems and Control Division*, DSC-Vol 57-2, ASME, New York, pp. 623-630.

Ellis, R.E., Ismaeil, O.M., Lipsett, M.G., 1993, "Design and evaluation of a high performance prototype planar haptic interface," *Advances in Robotics, Mechatronics, and Haptic Interfaces*, DSC-Vol 49, ASME, New York, pp. 55-64.

Faye, I.C., 1986, *An Impedance Controlled Manipulandum for Human Movement studies*, M.S. thesis," Mech. Eng. Dept., M.I.T., Cambridge, MA.

Goertz, R.C., and Thompson, W.M., 1954, "Electronically controlled manipulator," *Nucleonics*, 46-47.

Gosselin, C., and Angeles, J., 1989, "The optimum kinematic design of a spherical three-degree-of-freedom parallel manipulator," *ASME J. Mech., Trans., and Automation in Design*, *111*, 202-207.

Hayward, V., 1995, "Toward a seven axis haptic device," *Proceedings 1995 IEEE/RSJ Int. Conf. Intelligent Robots and Systems*, Vol. 3, Pittsburgh, PA, pp. 133-139.

Hirata, Y., and Sato, M, 1992, "3-dimensional interface device for virtual work space," *Proceedings, IEEE Int. Conf. on Intelligent Robots and Systems*, Raleigh, NC, pp. 889-896.

Hui, R., Ouellet, A., Wang, A., Kry, P., Williams, S., Vukovich, G., and Perussini, W, 1995, "Mechanisms for haptic feedback," *Proceedings, IEEE Int. Conf. Robotics and Automation*, Nagoya, Japan, pp. 2138-2143.

Hunter, I.W., Doukiglou, T.D., Lafontaine, S.R., Charette, P.G., Jones, L.A., Sagar, M.A., Mallinson, G.D., and Hunter, P.J., 1994, "A teleoperated microsurgical robot and associated virtual environment for eye surgery," *Presence*, *2*, 265-280.

Iwata, H., 1990, "Artificial Reality with force-feedback: development of desktop virtual space with compact master manipulator," *Computer Graphics*, *24*, 165-170.

Jacobsen, S.C., Smith, F.M., Backman, D.K., and Iversen, E.K., 1991, "High performance, high dexterity, force reflective, teleoperator II," *Proceedings, ANS Topical Meeting on Robotics and Remote Systems*, Albuquerque, NM.

Jacobus, H.N., Riggs, A.J., Jacobus, C.J., and Weinstein, Y., 1992, "Implementation issues for telerobotic handcontrollers: human-robot ergonomics," M. Rahimi and W. Karkowski, ed., *Human Robot Interaction*, Taylor and Francis, London, pp. 284-314.

Jau, B.M., 1992, "Man-equivalent telepresence through four fingered human-like hand system," *Proceedings, IEEE Int. Conf. Robotics and Automation*, Nice, pp. 843-848.

Kazerooni, H., 1995, "The human power amplifier technology at the University of California, Berkeley," *Proceedings, ASME Dynamic Systems and Control Division*, DSC Vol 57-2, ASME, New York, pp. 605-613

Lindemann, R., and Tesar, D., 1989, "Construction and demonstration of a 9-string six dof force reflecting joystick for telerobotics," *Proceedings, NASA Conference on Space Telerobotics*, Vol. 4, JPL Publication 89-7, pp. 55-63.

Marco, D., Torfason, L., and Tesar, D., 1989, "Computer simulation and design of a three degree-of-freedom shoulder module," *Proceedings, NASA Conference on Space Telerobotics*, Vol. 5, JPL Publication 89-7, pp. 273-282.

Marshall, W.C., DeMers, R.E., Schipper, B.W., and Levitan, L., 1993, "Synergistic computing applied to a virtual-pivot six-degree-of-freedom hand controller designed for aerospace telerobotics," *Proceedings, AIAA Computing in Aerospace IX*, San Diego, CA, AIAA 93-4506.

Massie, T.H., and Salisbury, J.K., 1994, "The PHANToM haptic interface: a device for probing virtual objects," *Dynamic Systems and Control 1994*, DSC-Vol 55-1, ASME, New York, pp. 295-301.

Millman, P.A., Stanley, M., and Colgate, J.E., 1993, "Design of a high performance haptic interface to virtual environments," *Proceedings, IEEE Virtual Reality Annual International Symposium*, Seattle, WA, pp. 216-222.

Ouerfelli, M., and Kumar, V., 1994, "Optimization of a spherical five-bar parallel drive linkage," ASME J. Mech. Design, *116*, pp. 166-173.

Mosher, R.S., 1967, "From Handyman to Hardiman," *Society of Automotive Engineers Trans.*, *76*, 588-597.

Noll, A.M., 1971, *Man-Machine Tactile Communication*. Ph.D. dissertation, Elect. Eng. Dept., Polytechnic Institute of Brooklyn.

Ramstein, C., and Hayward, V., 1994, "The Pantograph: a large workspace haptic device for a multi-modal human-computer interaction," *CHI'94, Conf. on Human Factors in Computing Systems ACM/SIGCHI*, Boston, MA.

Salcudean, S.E., Wong, N.M., and Hollis, R.L., 1995, "Design and control of a force reflecting teleoperation system with magnetically levitated master and wrist," *IEEE Trans. Robotics and Automation, 11*, 844-858.

Salisbury, J.K., and Craig, J.J, 1982, "Articulated hands: force control and kinematic issues," *Int. J. Robotics Research*, *1*, 4-17.

Sutherland, I.E., 1965, "The ultimate display," *Proceedings, IFIP Congress 65*, New York, pp. 506-508.